

Direct measurement of the damping and stiffening capabilities of cylindrical underplatform dampers

Original

Direct measurement of the damping and stiffening capabilities of cylindrical underplatform dampers / Gastaldi, C.; Berruti, Teresa M.. - In: MECHANICAL SYSTEMS AND SIGNAL PROCESSING. - ISSN 0888-3270. - 139:106632(2020), pp. 1-15. [10.1016/j.ymsp.2020.106632]

Availability:

This version is available at: 11583/2786626 since: 2020-02-14T11:05:07Z

Publisher:

Elsevier

Published

DOI:10.1016/j.ymsp.2020.106632

Terms of use:

This article is made available under terms and conditions as specified in the corresponding bibliographic description in the repository

Publisher copyright

Elsevier postprint/Author's Accepted Manuscript

© 2020. This manuscript version is made available under the CC-BY-NC-ND 4.0 license
<http://creativecommons.org/licenses/by-nc-nd/4.0/>. The final authenticated version is available online at:
<http://dx.doi.org/10.1016/j.ymsp.2020.106632>

(Article begins on next page)

Direct measurement of the damping and stiffening capabilities of cylindrical underplatform dampers

C. Gastaldi^{a,*}, Teresa M. Berruti^a

^aPolitecnico di Torino, Corso Duca degli Abruzzi 24, 10129, Torino, Italy

Abstract

The paper focuses on the cylindrical underplatform damper, a friction damping device widely used in power generation turbines. **The first goal of the paper is to estimate the stiffness and damping contribution of cylindrical dampers interposed between adjacent blades vibrating along a typical in-phase mode. For the first time, the damper characterization is performed through the direct measurement of contact forces and platform displacements.**

Measurements show that the damper does not introduce damping **or** stiffness if the two platforms, with which the damper is in contact, share the same angles (**i.e. blade with symmetrical platform**) and are vibrating in-phase. This is an adequate design choice if **only the** damper sealing function is required, while changes to the disk dynamics are not desired. The damper produces a small stiffening effect only if the two adjacent platforms have different angles. These findings are confirmed by an analytical derivation performed on the basis of a simple yet effective damper model.

The damper numerical model requires **parameters which may be calibrated**, i.e. the cylinder-on-flat tangential contact stiffness. **The second goal of the paper is to use the experimental evidence on contact forces and platform displacements to estimate these parameters** for different centrifugal loads using a purposely developed technique. These values are compared with those obtained at **an identically designed contact interface on a curved flat damper** (i.e. cylindrical damper with a flattened side). The differences found **in the calibration parameters** show that the local stiffnesses depends not only on the local geometry of the contact but also on the damper kinematics.

Keywords: friction, damping, turbine, contact stiffness, cylindrical damper

1. Introduction

The dynamic design of turbine stages has improved over the years by introducing, in numerical models, the contribution of friction present between the contact interfaces of the different components. Friction contacts can occur between parts integral to the blades such as shrouds or interlocked tip platforms [1, 2, 3, 4, 5, 6, 7, 8, 9], or, between blades and separate devices such as underplatform dampers (UPDs) [10, 11, 12, 13, 14, 15, 16, 17, 18, 19].

Underplatform dampers are small prismatic bodies inserted between **the base/ platforms supporting the** blades, kept in contact with the blades' platforms by centrifugal force. The dynamic design of blades with UPDs has been deeply studied over the past 15 years. The UPDs have been designed both as "solid dampers" of various shapes, (cylindrical, curved-flat, wedge) [20, 21, 22, 23, 24, 25, 26, 27, 28], and as thin and highly deformable dampers, namely strip dampers or sealing strips [29, 30, 31, 32]. **One of the main objectives in this field is to characterize the damper behaviour, either numerically or experimentally, in terms of its stiffening and damping effect on the blades' dynamic response [33, 34, 35, 36, 17, 19, 27]. An alternative approach to this characterization represents the damper effect in terms of blade platform-to-platform hysteresis cycles [37, 51].**

In the literature, the experimental activity on UPDs focuses on two main lines of research: 1) the determination of contact parameters and 2) the measurement of the forced response of blades with UPDs. The test rigs of the first line of research measure the quantities of interest (forces and displacements related to the contact) on one single contact

*Corresponding author

Email address: chiara.gastaldi@polito.it (C. Gastaldi)

[33, 38, 39, 40, 41, 42, 43]. The limit of this test rigs is that, focusing on a single contact, they **usually apply a constant preload (simplified assumption) and they** might not reproduce the real relative displacement conditions at the contact. The second line of research test rigs may include one to two blades([19, 11, 44, 45, 46, 47, 48], or a non-rotating bladed disk [15], or even rotating bladed disks [49, 16].

The research group to which the authors of this paper refer, has introduced since 2010 [44] a third research line, namely the measurement of contact parameters directly on the UPD itself, **thus taking into account the component kinematics and its complex loading conditions**. The first test rig, which carries out this type of measurement, the so called first Piezo Damper test rig, is described in [50] and more in detail in [37]. This test rig is based on the principle that the relative displacement of the moving blade platforms imposes kinematics to the UPD. Thus, giving as input the real relative displacement of the platforms, it is possible to obtain and measure realistic UPD kinematics. Furthermore, the measurement of forces and displacements at the damper-platform interface allows the contact parameters and the overall dissipated energy to be determined. In this kind of test **rig** a laser head measures damper displacements and rotation, relating them to platform displacements and contact forces. This dedicated experimental evidence was, and still is, believed to be the most accurate way to determine contact parameters (tangential contact stiffness, friction coefficients) for the UPDs. The same concept has been **used** more recently in [19] and [26].

The experimental results obtained with this type of test rigs focus on the damper kinematics, allowed the authors of this paper to develop a technique to optimize the damper shape and the angles of the blade platforms [37, 51, 52].

In this paper the authors put to good use the experience accumulated in the past to characterize a particular form of UPD: the cylindrical UPD. Cylindrical UPDs are in fact still of great interest since they are widely used particularly in power generation turbines. Their simple shape can in fact easily be manufactured with relatively low costs. Furthermore, the cylindrical damper has the advantage of adapting to all blade platform angles.

A new version of the previous test rig is used here. In this new experimental setup, as in the previous ones [37], contact forces, local displacements and damper rotation are directly measured by imposing a relative displacement at the two platforms. Unlike its predecessor it is now possible to reach frequencies and **contact force per length of contact** of the same order of magnitude of those of real UPDs working conditions[53]. Furthermore, unlike single contact test arrangements, the test rig is able to unveil the influence of contact interface kinematics, normal load variation during the cycle, etc.

In detail, the paper is organized in sections divided as follows. Section 2 describes the relative displacement of the blade platforms, particularly in the case considered here where the blades vibrate in-phase. Section 3 gives a description of the new test rig and its experimental capabilities. Section 4 describes the typical measurement output in terms of hysteresis cycles and damper rotation in the case of a cylindrical damper in contact with symmetrical platforms. The negligible contribution in terms of stiffness and damping introduced by the damper are discussed. Section 5 proposes a simple yet effective cylindrical damper model capable **of** reproducing the negligible effect of the damper detailed in Sect. 4. The model is then used to predict which changes in the experimental set-up are needed in order to improve the damper stiffening effect. In detail, the platform angles are changed in order to ensure that the left and right damper-platform contact points lie at a different distance from the damper center of mass. The predictions of the model are then verified experimentally in Section 6. Section 7 presents an ad-hoc procedure for the determination of contact stiffness values for cylindrical dampers. The values from the experimental campaign exploring increasing centrifugal loads are shown as a function of the normal load at the contact. These values are compared with those obtained on a damper with the same radius but with a flattened side (i.e. curved-flat damper).

2. The kinematics of the blade platforms

The UPD can be seen as a rigid body placed between the platforms of the blades, **which, in turn, drive its motion**. The relative motion of the platforms drives the damper to move with a certain kinematics. This kinematics is important since it influences the dissipative capability of the damper. Once the relative motion of the platforms has been set, each damper of different geometry will have a different kinematics and therefore a different dissipative capability.

To reproduce the UPD kinematics in a laboratory setting, a test rig is necessary to simulate the relative displacement of the platforms in contact with the damper. In the case of blades vibrating in-phase along a bending mode (one of the most common occurrences), the relative motion of the platforms is vertical as shown in Fig.1. The test rig should then impose a vertical displacement between the two platforms. Since it is the relative displacement that counts, the right platform can be kept fixed while the vertical displacement is entirely imposed on the left platform as shown in

the scheme of Fig. 2. The test rig **briefly** described in the next section is designed to impose this relative displacement to two rigid bodies acting as platforms. At the same time the rig measures displacements and rotation of the damper together with displacements and forces at the damper-platform contact. **All measured and derived quantities shown in the present work come with uncertainty bands $\leq 2\%$. The reader is referred to [54] for a thorough description of the rig, the design choices and a thorough error analysis.**

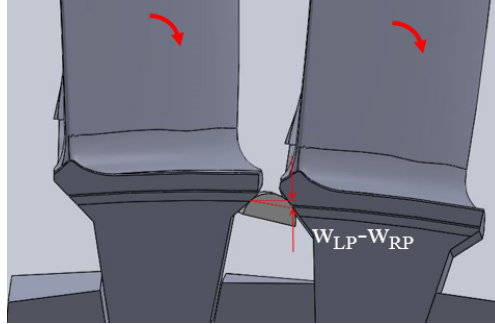


Figure 1: Absolute kinematics of two adjacent blades vibrating in-phase along a bending mode and resulting relative blade platform displacement $w_{LP} - w_{RP}$, parallel to the direction of the centrifugal force on the damper

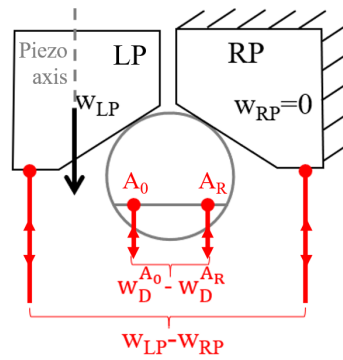


Figure 2: Scheme representing the relative platform motion $w_{LP} - w_{RP}$ in vertical direction (radial, parallel to the centrifugal force) during a typical in-phase bending mode. The red lines represent the differential laser head position used to measure different kinematic quantities: $w_{LP} - w_{RP}$ is the platform relative vertical displacement signal, while $w_D^{A_0} - w_D^{A_R}$ is the signal used to estimate damper rotation.

3. The test rig

The test rig shown in Fig.3a-b is composed of three main parts:

1. Left platform: a moving part connected to the **P-216 PICA Power** piezo actuator which imposes a sinusoidal motion parallel to the piezo axis¹;
2. Right platform: a fixed part which is connected to the two force sensors measuring the contact forces between the damper and the platform on the right side;
3. Underplatform damper: the prismatic body kept in contact with the two platforms wires connected to dead weights simulating the centrifugal force.

¹A parallel mechanism composed of two flexural hinges is chosen to guide the motion of the piezoactuator due to its adequate resolution, low level of parasitic forces, motion smoothness and zero backlash. The inevitable coupling between degrees of freedom is proportional to the ratio between the amplitude of imposed displacement and the length of the flexural hinge, as demonstrated in [50]. In the present case the error due to coupling is at most $\approx 0.1\%$ (imposed displacement $\leq 30 \mu\text{m}$ and 25 mm long flexural hinge).

In the case described here the test rig is mounted so that the actuator imposes a displacement in the vertical direction, as in Fig. 2, so as to reproduce a typical in-phase bending mode. It is worth noting that in a real turbine stage the relative motion will still be parallel to the centrifugal force on the damper (i.e. radial orientation centered at the damper center of mass) provided that the damper-platform contacts share the same distance with respect to the blade neck axis. The assembly of the rig can be modified to investigate the out of phase bending mode (i.e. circumferential/horizontal platform relative motion), should it be of interest [54].

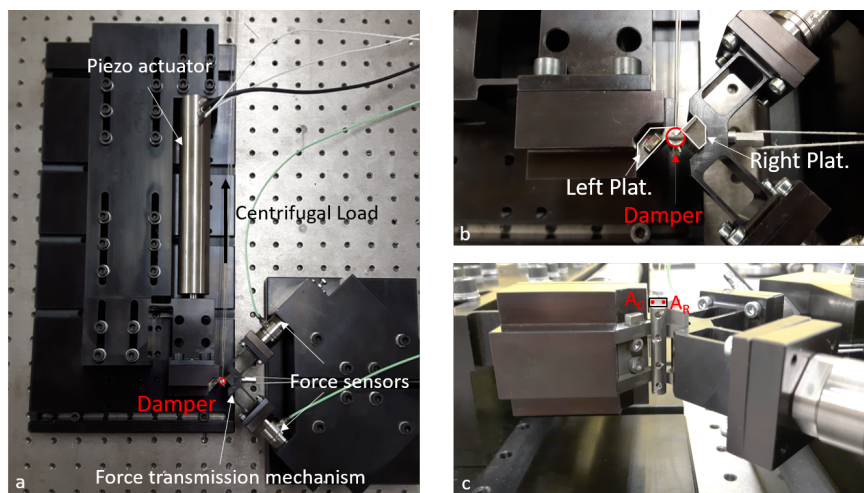


Figure 3: a. Top view of the test rig. b. Close-up top view of the test rig. c. Front view of the test rig, focus on the damper and surrounding platforms. The top portion of the damper has been machined to produce a flat surface used to point the differential laser (points A_0 and A_R) and measure the damper rotation as shown in Fig. 2.

3.1. The force measurement

As shown in Fig. 3a, the force is measured through a measuring device with two arms, each consisting of two parallel plates, connected to the right platform. The two arms, perpendicular to each other, transmit the force to two **Kistler 9323AA** force sensors. Each of the two sensors measures a component of the total force exchanged between the damper and the right platform. The geometry of the arms is designed as a parallelogram to allow for high rigidity along the axis of the arm and high flexibility in the transverse direction (axial to transverse stiffness ratio >100). This solution allows the force measurement to be decoupled. Each sensor receives the force component along the direction of the axis of the arm to which it is connected. The proposed geometry was chosen after an accurate analysis to be able to reach sufficiently high frequencies and, at the same time, to decouple the force on the two sensors. More details about this matter can be found in [26].

3.2. The displacement and rotation measurement

The sinusoidal relative displacement in vertical direction of the left platform LP with respect to the right one RP ($w_{LP} - w_{RP}$) is measured by a **Polytec OFV-512** differential laser head pointing to the bottom of the two platforms as shown in Fig. 2. The damper rotation is obtained by pointing the differential laser at two points, here termed A_0 and A_R , as shown in Fig. 2. To this purpose the upper portion of the damper is purposely machined as shown in Fig. 3c to produce a flat surface necessary to reflect the laser signals. Being A_0 and A_R the two points and $w_D^{A_0}$ and $w_D^{A_R}$ the corresponding displacements measured by the laser (Fig. 2), the damper rotation is obtained as $\beta = \frac{w_D^{A_R} - w_D^{A_0}}{A_0 A_R}$.

3.3. A typical measured hysteresis cycle

A typical diagram that can be obtained from the measurements of the test rig is the *Platform-to-platform hysteresis cycle*. Three examples of such a diagram obtained from an optimized curved-flat damper[25] for increasing relative platform displacements are shown in Fig.4. The x axis of the hysteresis cycle shows the relative platform displacement

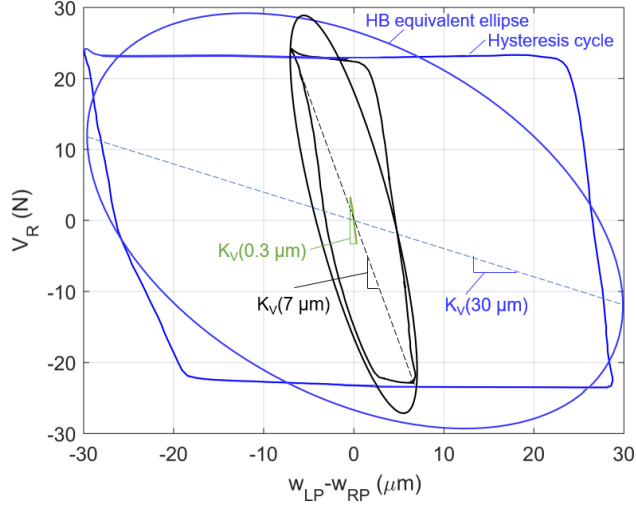


Figure 4: Typical curved-flat damper hysteresis cycles and corresponding HBM equivalents for different amplitudes of imposed platform displacement w^C : $30 \mu\text{m}$ (blue), $7 \mu\text{m}$ (black) and $0.3 \mu\text{m}$ (green).

($w_{LP} - w_{RP}$) over one period of vibration (mono-harmonic sinusoidal signal $w_{LP} - w_{RP} = w^C \cdot \cos(\omega t)$). The y axis of the diagram shows the component of the contact forces on the right platform (the platform connected to the force sensors) aligned with the relative platform displacement during one period of vibration. In fact, only the component of the force parallel to the displacement, will account for dissipated energy and stiffening. In case of in-phase vibration the force component is the vertical one, here termed V_R .

In Fig.4 the hysteresis cycles are shown together with their Harmonic Balance (HB) equivalent ellipses [55]. The ellipses are obtained simply by substituting the force signal V_R with its first harmonic component $V_R^C \cdot \cos(\omega t) + iV_R^S \cdot \sin(\omega t)$. One interesting property of the HB ellipse is that it shares the same area (i.e. dissipated energy) as the original cycle. **If fact, due to the orthogonality of the exponential functions representing the different harmonic contributions ($e^{-i\omega m t} \cdot e^{-i\omega n t} = 0$ if $m \neq n$), it can be demonstrated that, if the platforms imposed displacement is assumed to be mono-harmonic, then only the first harmonic component of the contact force will contribute to energy dissipation.** Furthermore the global stiffening effect introduced by the damper between the platforms can be computed as follows:

$$K_V = \frac{V_R^C}{w^C} \quad (1)$$

and is represented graphically using dashed lines in Fig. 4.

The platform-to-platform hysteresis cycle has the advantage of showing simultaneously, the damping effect (i.e. area inside the cycle) and the stiffening effect (K_V) introduced by the damper between the platforms, regardless of the number and geometry of the contact interfaces. Furthermore its shape gives an indication on the damper behaviour[52]. The shape of the $30 \mu\text{m}$ cycle shown in blue in Fig. 4 is regular and typical of a highly efficient stick-slip pattern, usually found with considerable imposed relative platform motion (i.e. $w^C > 20 \mu\text{m}$). As the imposed platform motion decreases the dissipated energy (cycle area) decreases while the global stiffness K_V increases. If the platform imposed motion decreases below a limit level ($0.3 \mu\text{m}$ cycle in Fig. 4), the damper is fully stuck between the platforms (no sliding), then K_V is at its maximum.

4. The Platform-to-platform hysteresis cycle for a cylindrical damper

In Fig.5a the hysteresis cycle obtained for a cylindrical damper between two symmetric ($45^\circ - 45^\circ$) platforms is compared to an hysteresis cycle of a high performing curved-flat damper [53]. Both damper cross section shapes are depicted in Fig. 5c. It can be noticed that, compared to the curved-flat damper cycle, the cylindrical damper cycle is compressed on a line and therefore displays a negligible inner area, i.e. no dissipated energy. Furthermore the cycle/line appears almost horizontal. This indicates that the cylindrical damper's contribution to stiffness (i.e. K_V)

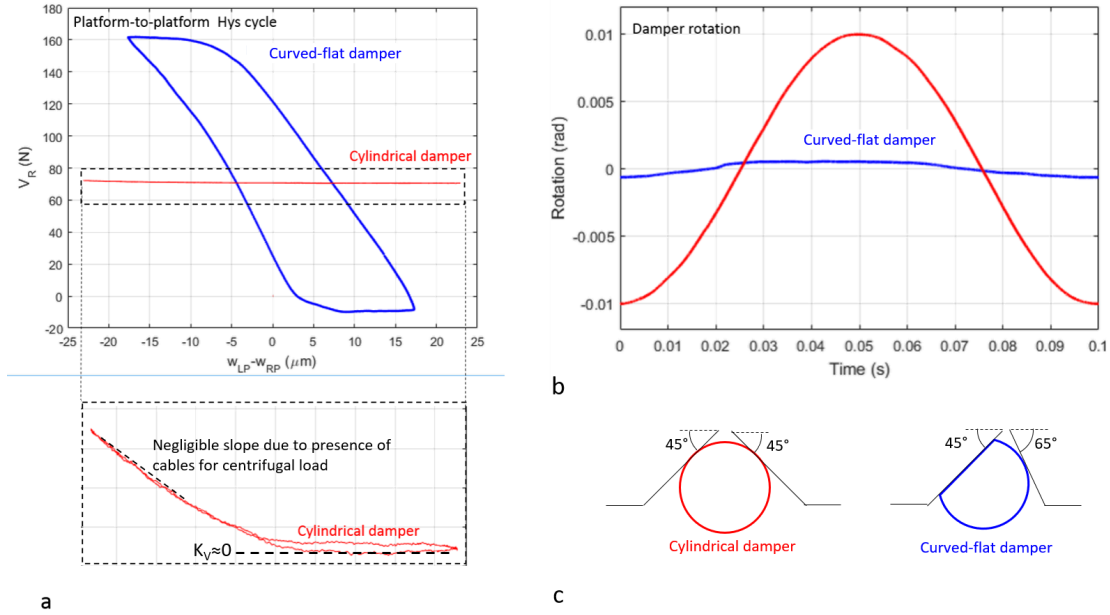


Figure 5: a Platform-to-platform hysteresis cycles b Damper rotation c Damper cross section shape: a comparison between curved-flat and cylindrical dampers. Signals recorded at $f= 100$ Hz, centrifugal load $CF= 15$ kg.

is also negligible, as also observed in the lower blade response level in [35]. The cause of this poor contribution to stiffness and damping, is to be found in the damper-platform kinematics. In fact the cylindrical damper in Fig. 5c does not slide, rather it rotates **around its center of mass** between the platforms. This statement is proven by the measurement of the damper rotation depicted in Fig.5b. The rotation of the curved-flat damper is lower than 1 mrad, while the rotation of the cylindrical damper is more than one order of magnitude larger, up to 20-30 mrad. The damper contact points at

By zooming in on the cylindrical damper hysteresis cycle (lower portion of Fig. 5a), the reader may notice that the left-most portion of the hysteresis cycle exhibits a minor slope (still two orders of magnitude lower than K_V values typically associated with curved-flat dampers). This minor slope should however be disregarded as it is most likely caused by the presence of the cables used to apply the centrifugal load which prevent the damper from rotating freely. This hypothesis is corroborated by the fact that this slope changes slightly if cables are re-arranged.

4.1. The influence of experimental boundary conditions

The low-dissipation low-stiffening trend of the cylindrical damper is consistent for a variety of experimental boundary conditions. The shape of the platform-to-platform hysteresis cycles does not vary for different values of centrifugal load, as shown in Fig.6a². As depicted in Fig.6b, the rotation signal remains unchanged as well. In fact the four different rotation measurement signals, obtained for increasing values of centrifugal load, are overlapped. This means that the amount of rotation does not depend on the centrifugal load. The influence of the excitation frequency and that of the amplitude of imposed displacement are also explored. As shown in Fig.6c the shape of the cycle does not change for different frequencies or different displacement amplitude. **The 250 Hz loop is displaying the same $K_V \approx 0$ slope and the same influence of the cables as the 100 Hz loop. The high frequency oscillations visible on the 250 Hz loop are produced by the force measurement mechanism which is drawing closer to its internal resonance. It is worth noting that these oscillations would be unnoticeable on a hysteresis cycle of a typical curved flat damper (i.e. force amplitude excursion > 10 N).**

²The reader will notice that the mean value of V_R understandably changes with increasing values of CF . It should be noted that in the following figures the mean component of V_R may have been removed in order to perform more straightforward comparisons between different platform-to-platform hysteresis cycles

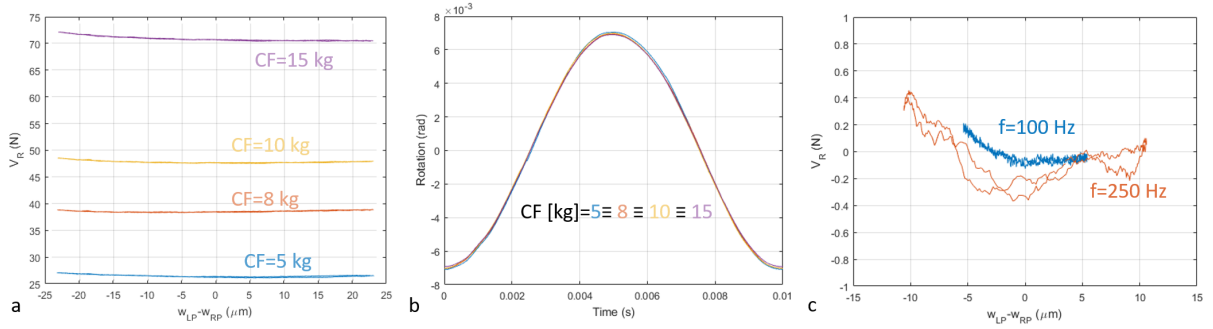


Figure 6: a Platform-to-platform hysteresis cycles b damper rotation of a cylindrical damper for increasing values of centrifugal force CF, $f = 100$ Hz C. c Platform-to-platform hysteresis cycles recorded at CF=15 kg for increasing values excitation frequency f .

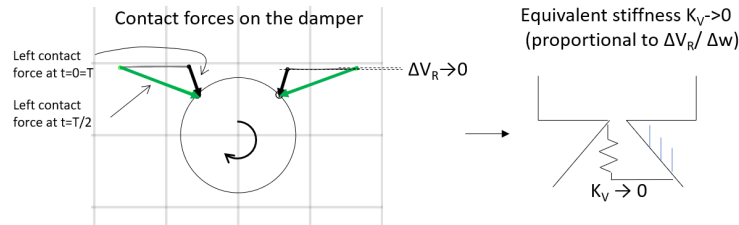


Figure 7: (Left) Scheme of the variation of the vector of the friction forces at the damper platform interface. In black forces at time $t = 0 = T$ and in green forces at time $t = \frac{T}{2}$ where T is the period of vibration. (Right) Equivalent stiffness in vertical direction.

4.2. Platform-damper kinematics influence the damper performance

The results of the experimental campaign on the cylindrical damper supported by two symmetrical $45^\circ - 45^\circ$ platforms confirms that the damping and stiffening effects usually expected of a damper are here not present. This is caused by a combination of factors. The purely vertical motion of the platforms and the symmetrical position of the damper-platforms contact points with respect to the damper center of mass cause the damper to undergo a pure rotation without sliding. The lack of sliding is further confirmed by the ratio between the tangential and normal component of the contact forces (here not shown for brevity), which never reaches the gross slip limit. **Another indication of the damper "pure" rotation around its center of mass is the lack of relative motion between the damper center of mass and the left platform, i.e. the signal measured with the differential laser has an amplitude $< 0.5 \mu\text{m}$ for a platform motion of $w^C = 30 \mu\text{m}$.**

The "pure" rotation of the damper around its center of mass has consequences on the local kinematics at the contact. With reference to Fig. 8, it can be observed that, in the case of a rotating cylindrical damper, the physical point on the damper initially in contact with the platform does move out of the contact area, however the contact point does not move along the platform, i.e. no gross sliding. On the other hand, if one considers a curved flat damper (with negligible rotation), it can be seen the physical point on the damper initially in contact with the platform never moves out of the contact area, and the damper-platform contact point move along the platform (i.e. gross sliding). The pure and unrestrained rotation the damper undergoes affects the direction of the platform-damper contact forces represented in Fig.7. The force vectors depicted on the right contact represent the resulting measured contact force in amplitude and direction. The vectors on the left are derived from those on the right by equilibrium with the centrifugal force, as further explained in [37]. Even if the resultant contact force on each side varies its direction during a cycle, it can be observed that the vertical component of the contact force (V_R) does not change ($\Delta V_R = 0$). **Only the force components aligned (parallel) to the platform relative motion can contribute to stiffness (see Eq. 1) and dissipate energy (the work of a force is the scalar product of the force and the corresponding displacement, i.e. the product of the displacement and the force component parallel to it). Therefore, the damper will have negligible effect on the disk**

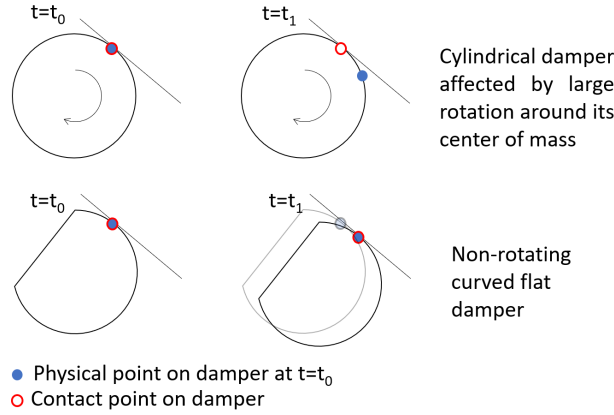


Figure 8: Kinematics at the contact in case of a rotating cylindrical damper and of a non-rotating curved-flat damper.

frequency response function both in terms of dissipation and frequency shift (stiffening) (i.e. inter-platform stiffness and damping ≈ 0).

It can therefore be concluded that, in case of pure in-phase blade vibration, cylindrical dampers supported by symmetric platforms will provide only a sealing function but will not affect the dynamic response of the surrounding disk. A similar set of observations holds for cases close to the ideal one considered here, e.g. blades vibrating with a phase shift not null but fairly close to zero (i.e. $< 10^\circ$). In those cases, a small circumferential (horizontal) relative displacement will be present (typically one order of magnitude lower than the vertical motion) and the influence of the cylindrical damper will still be low enough as to be considered negligible.

5. An effective and simple damper model

As shown in Fig. 8 and confirmed by the experimental evidence, the damper rotates about its center of mass and remains in full stick condition (i.e. no relative tangential motion between damper and platform contact points). In this case, if one wishes to represent the damper-platform contact elasticity using springs[56], similarly to the model shown in Fig. 9, K_V can be expressed as a function of the contact springs k_n and k_t and of the platform angles θ_L and θ_R :

$$K_V = f(k_n, k_t, \theta_L, \theta_R) \quad (2)$$

The procedure used to derive the K_V is full recounted in Appendix A. With reference to the analytical expression of K_V in Eq. A.9, if $\theta_L = \theta_R$, then $K_V = 0$ regardless of the numerical value of platform angles and contact stiffness. This constitutes an analytical proof of the un-effectiveness of a cylindrical damper with symmetrical platforms in case of pure in-phase vibration.

A further proof of the soundness of the model presented here is given by considering the experimental evidence shown in [26]. In it, a non-zero equivalent stiffness is obtained for a cylindrical damper in contact with two asymmetrical platforms whose relative displacement is far from the pure vertical displacement encountered in case of in-phase vibration. The model described fully confirms these findings.

It should be noted that the K_V expression holds in the case of full stick condition and is used in this paper to estimate contact stiffness values (see Sect. 7.3) starting from experimental evidence coherent with the full stick assumption. However the model shown in Fig. 9 takes into account gross sliding and can therefore be used without limitations.

6. Cylindrical damper with different platform angles

According to the damper model described in Sect. 5, the stiffening effect introduced by the damper, negligible if adjacent platforms vibrating in-phase have the same inclination $\theta_L = \theta_R$, should become non-negligible if platforms with different angles are used. To verify this hypothesis a similar set of measurements is performed on the same

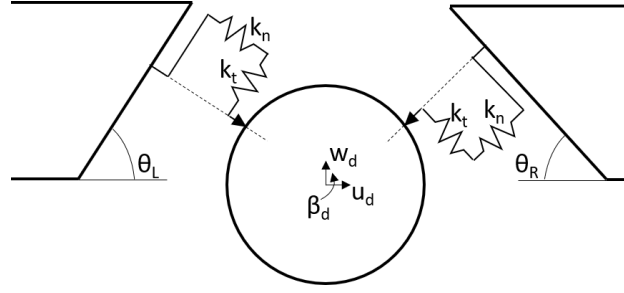


Figure 9: Model of a cylindrical damper between two adjacent platforms. The damper is here considered as a rigid body and the contact elasticity is modeled using simple springs.

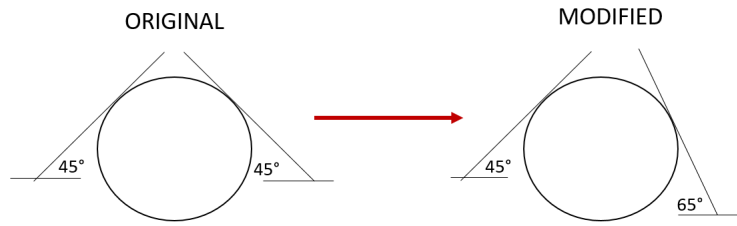


Figure 10: Platform angles in original and modified configuration

damper between platforms with two different angles $\theta_L = 45^\circ - \theta_R = 65^\circ$.

It can be seen from Fig.11 that the hysteresis cycle obtained for the damper in contact with the platforms $45^\circ - 65^\circ$ is inclined with respect to the cycle obtained with the symmetrical platforms ($45^\circ - 45^\circ$) which is almost horizontal. The average inclination of the cycle (K_V in Fig.11), as previously seen, is a measure of the stiffening effect introduced by the damper in the direction of the relative motion of the platforms (in this case the vertical direction).

This means that a cylindrical damper is capable of introducing stiffness between adjacent blades vibrating in-phase only if the corresponding platforms have different inclination angles.

The measurement is repeated imposing a greater relative displacement to the platforms, the resulting hysteresis cycle is visible in Fig.12. It can be noted that:

- despite the increased platform motion the damper does not reach gross slip condition, the area inside the cycle is limited and compatible with a microslip regime;
- the slope of the cycle remains unchanged, i.e. the stiffening effect does not vary significantly;
- the cycle appears more irregular, i.e.the force signal disturbed, due to the increased rotation of the damper in the event of greater displacement of the platforms.

In order to have cleaner signals, it was decided to perform the measurements for limited values of imposed platform relative displacement ($\pm 5-6\mu m$). Furthermore, it is possible to filter the force signal and retain only its first harmonic component, as discussed in Sect. 3.3.

The effect of the centrifugal load on the platform-to-platform hysteresis cycle and resulting K_V value is shown in Fig.13. The K_V slope increases with the centrifugal force. With reference to Eq. 2, since the experimental evidence comes from a unique damper-platforms configuration ($\theta_L = 45^\circ - \theta_R = 65^\circ$), it can be concluded that the contact stiffness values k_n and k_t are affected by the centrifugal load, i.e. contact pressure.

7. Estimation of contact parameters

According to the state of the art model shown in Fig. 9, each flat-cylinder (damper-platform) contact is characterized by a friction coefficient μ , a stiffness normal to the platform contact surface k_n and by k_t , stiffness tangential to the

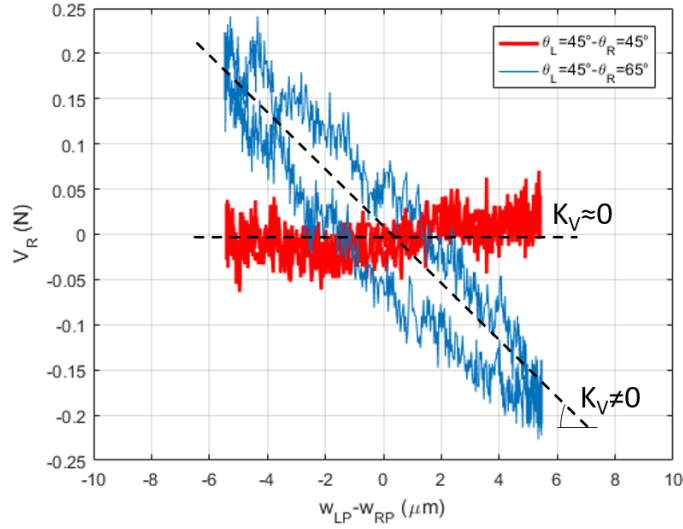


Figure 11: Platform-to-platform hysteresis cycles for cylindrical damper in contact with 45°- 45° platforms and 45°- 65° platforms, centrifugal load CF= 15 kg, $f= 100$ Hz.

platform. In order to build a model capable of trustworthy predictions, it is necessary to correctly estimate the value of the contact parameters[57].

7.1. Friction coefficient

Friction coefficients are typically estimated through the tangential/normal contact force ratio measured for one period of vibration [37]. If the ratio keeps constant in time and is equal to a maximum, than the ratio is set equal to μ . In the present case gross slip is never reached and, consequently, the tangential/normal force ratio is continuously varying over the period of vibration and never reaches values larger than 0.2. It is therefore impossible to estimate μ , one can only confirm that μ will be larger than 0.25.

7.2. Normal contact stiffness

The normal contact stiffness k_n of a steel cylinder on flat contact can be easily obtained from interpolations of experimental data on rolling bearings [58], later confirmed by Brändlein's theoretical investigations based on Hertz theory [59]. Both formulas express k_n as a function of the elastic characteristics of the material, the contact length and the normal contact load. It is worth noting that, in the present case, the contact length is tightly controlled thanks to the shape of the platform inserts (two 4 mm long contact pads) shown in Fig. 3c.

7.3. Tangential contact stiffness

In the case of curved flat-dampers, the tangential contact stiffness k_t has been successfully measured by relating the tangential contact force to the corresponding tangential relative displacement at the contact measured using the differential laser head. This procedure cannot be carried out in the present case, as the large rotation undergone by the damper would pollute the laser reading of the relative tangential displacement, as fully explained in [53]. Providing a successful estimate of the contact stiffness values is still possible. As discussed in Sect. 5, the global stiffness K_V is a function of the local contact stiffness k_n and k_t and of the inclination of the platforms θ_L and θ_R .

The tangential contact stiffness k_t is derived by combining the information on the platform angles, the k_n value derived as described above and the measured K_V value. The full algorithm can be found in Appendix A. It is worth noting that this procedure would be ineffective if the only experimental evidence available were the one obtained on a cylindrical damper in contact with symmetric platforms.

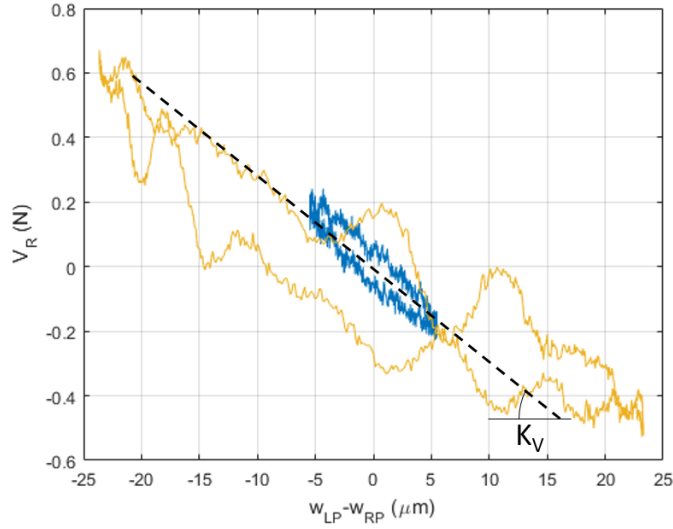


Figure 12: Platform-to-platform hysteresis cycles for a cylindrical damper in contact with 45°- 65° platforms, centrifugal load CF= 15 kg, different input motion amplitude.

7.4. A summary of results

Table 1 shows the stiffness values obtained for different centrifugal force values on the damper. The second column of the table shows the corresponding interval of variation of the normal contact load per unit length during the cycle. As expected, the total stiffness, but also the tangential and normal stiffness, increase with the increase of the normal load at the contact. It should be noted that the set of values shown in Table 1, unlike those in [26] where an equivalent oscillator is used in place of the damper, is exportable to other cases with different platform kinematics.

It can be observed that the normal contact stiffness values are orders of magnitude higher than the tangential ones, therefore they have negligible contribution to the global stiffening effect introduced by the damper. Figure 14 shows an experimental-numerical comparison. The numerical results have been obtained using the model shown in Fig. 9, fed with the contact parameters estimated as described in Sect. 7. The global stiffness K_V is captured correctly as it was used as a tuning parameter. The (negligible) damping contribution detected in the measured hysteresis loop may be due to microslip and partly to the presence of the centrifugal load wire. Microslip may be included by changing the contact model [60, 61], while the presence of the wire may be modeled by adding a rotational viscous damper. The most conservative choice (i.e. no damper and no microslip contribution) was here adopted as it was deemed more suitable for design purposes.

It is also interesting to compare the values of the tangential contact stiffness obtained for the cylinder-on-flat contact of two different dampers shown in Fig. 5:

- the cylindrical damper;
- the curved-flat damper analyzed in [54];

Both dampers are manufactured using the same material and share the same radius. In both cases the tangential contact stiffness at the cylinder-on-flat side is estimated starting from experimental evidence gathered using the test rig in Fig.3. The values of the tangential contact stiffness for the two dampers (versus the contact normal load per unit of length) are compared in Fig.15. The values pertaining to the cylindrical damper are those of Table 1, while the values referring to the curved-flat damper can be found in [54].

From Fig.15 it can be seen how the tangential contact stiffness for the same cylinder-plane contact is lower in the cylindrical damper case than in the curved-flat damper case. This difference is explained by analyzing the different kinematics at the contact during a cycle. The cylindrical damper tends to rotate, therefore the kinematics of the

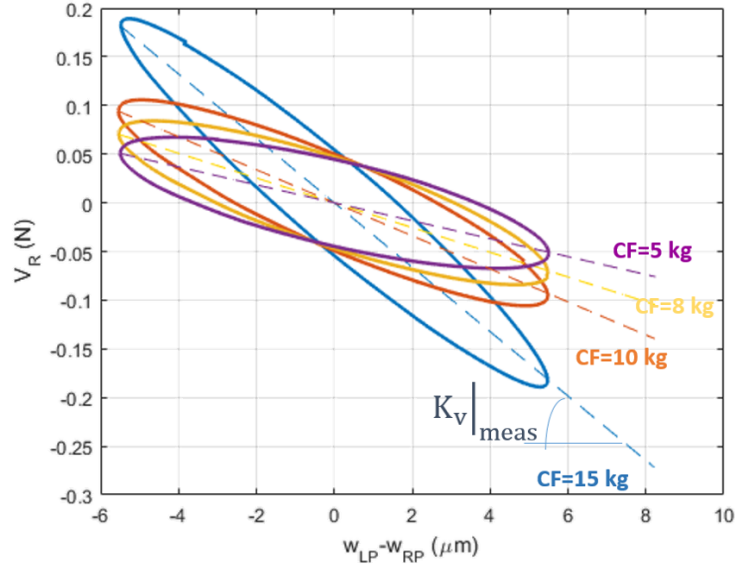


Figure 13: Platform-to-platform hysteresis cycles for a cylindrical damper in asymmetrical (45° - 65°) platforms, different centrifugal load values, $f= 100$ Hz.

Table 1: Contact stiffness values

CF (kg)	N/mm	K_V (N/ μ m)	k_n (N/ μ m)	k_t (N/ μ m)
5	5.6 - 7.5	0.0055 ± 0.002	227	0.1
8	8.8 - 11.3	0.011 ± 0.002	237	0.25
10	10 - 12.5	0.015 ± 0.002	239	0.35
15	13.8 - 17.5	0.031 ± 0.002	247	0.7

cylinder-plane contact is characterized by micro rotations of the cylindrical part. The curved-flat damper on the other hand, is "guided" by its flat portion in contact with the left platform and the relative motion at the cylinder-on-flat contact is a translation without any rotation. This difference in kinematics for the two types of damper can be observed from the rotation measurement shown in Fig.5b The rotation of the curved-flat is negligible compared to the rotation of the cylindrical damper.

The results of Fig. 15 therefore prove that, for the same local geometry of the contact (cylinder-on-flat), the tangential contact stiffness can be different depending on the local contact kinematics. In the event that the tangential relative displacement at the contact is also affected by rotation, the tangential contact stiffness is one order of magnitude lower than in a case of pure relative tangential translation.

8. Conclusions

Cylindrical dampers are still widely used especially in turbines mounted on turbo machines for power generation. The cylindrical shape in fact is cost-effective, easily manufactured and adaptable to any set of platform angles. This paper presents the results of a thorough experimental campaign aiming at evaluating the cylindrical damper contribution to blade vibration in terms of stiffness and damping. In detail, the paper focuses on the case where blades vibrate in-phase with each other according to a bending mode. This is in fact a typical mode of vibration of the blades excited by the gases during the turbine operation. Thanks to a test rig that allows for the simultaneous measurement of contact forces, relative platforms' displacement and damper rotation, the following main results have been reached.

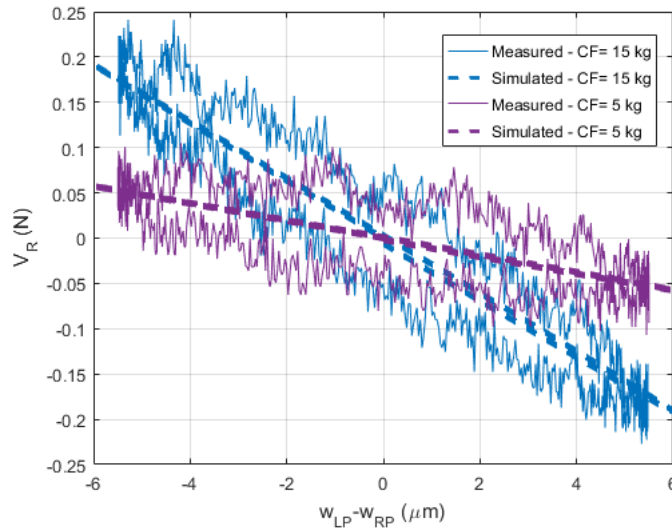


Figure 14: Experimental-numerical comparison of platform-to-platform hysteresis cycles for a cylindrical damper in contact with asymmetrical ($45^\circ - 65^\circ$) platforms, centrifugal load $CF= 5$ kg and 15 kg.

- The cylindrical damper, in contact with two symmetrical platforms, does not introduce any stiffening or damping effects. In this case, in fact, the damper rotates freely and the blades can move as if no damper were present.
- The cylindrical damper introduces a stiffening effect only if the angles of the two surrounding platforms are different from each other. In this case, in fact, the damper rotation is partially impaired and the damper partially constrains the relative movement of the platforms introducing a moderate platform-to-platform stiffness. The damping effect is still, similarly to previous case, negligible. In fact, the damper tends to rotate rather than slide on the platforms, and therefore does not generate an appreciable friction damping.
- In the case of cylindrical dampers in contact with two platforms with different angles, the local tangential stiffness of the cylinder-plane contact can be derived from the overall stiffness measurements. This stiffness proves to be much lower (about an order of magnitude) than that of the same cylinder-plane contact but with a damper that has the other side flattened.

These findings should help the designer in choosing the damper shape and the platform angles. If no additional stiffening and/or damping effect is needed, than a cylindrical damper with symmetric platforms will provide the required sealing function without introducing changes in the disk dynamics. On the other hand a cylindrical damper and two platforms with different angles will introduce a moderate stiffening effect. Finally, if stiffening and damping effects are needed, a curved-flat damper should be the preferred choice.

The damper theoretical model presented here evidences the analytical link, supported by experimental data, between turbine blade platform angles, mode of vibration and damper dynamic contribution. Furthermore the analytical derivation is used to estimate the tangential contact stiffness values starting from the experimental data. The contact stiffness values for different normal contact loads per unit length are here provided to be compared with other literature values but also to be directly used by designers. Contact stiffness values are in fact required by state-of-the-art non-linear codes as input values to compute the forced response of the blades with cylindrical dampers. **In this paper the contact stiffness values are fed to a numerical model of the damper between a set of platforms. This model, whose adequacy is verified against the in-phase case, can be used to explore other modes of vibration.**

Acknowledgments

The construction of the test rig presented in this paper has been funded within a research contract supported by Ansaldo Energia s.p.a.

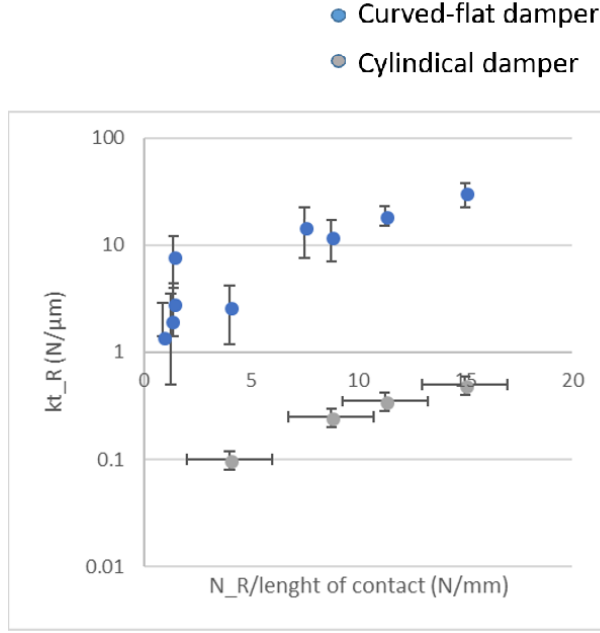


Figure 15: Tangential contact stiffness vs. the contact normal load per unit of length, for a cylinder-plane contact in a) a cylindrical damper and b) curved-flat damper.

Appendix A. Derivation of the global platform-to-platform contact stiffness

With reference to Fig. 9a, let us consider the in-plane equilibrium equations of a damper between a set of platforms with angles θ_L and θ_R .

$$M_D \cdot \ddot{Q}_D(t) = F_{CD}(t) + F_{ED} \quad (\text{A.1})$$

where $Q_D = (u_D, w_D, \beta_D)'$ is the vector of damper displacements, $F_{ED} = (0, CF, 0)'$ is the vector of external forces and F_{CD} is the vector of contact forces transported at the damper center of mass. In case of full stick condition Eq. A.1 can be re-written as:

$$M_D \cdot \ddot{Q}_D(t) + K_D \cdot Q_D(t) = K_P \cdot Q_P(t) + F_{ED} \quad (\text{A.2})$$

where $Q_P = (u_{LP}, w_{LP}, u_{RP}, w_{RP})'$ is the vector of platforms displacements (considered as an external information at this stage), and $[K_D]$ and $[K_P]$ are the contact stiffness matrices connected to damper and platforms respectively. The contact stiffness matrices can be expressed as:

$$\begin{aligned} K_D &= T' \cdot K_{local} \cdot T \\ K_P &= T' \cdot K_{local} \cdot R \end{aligned} \quad (\text{A.3})$$

where matrix K_{local} is diagonal and function of the contact stiffness values $K_{local} = \text{diag}(k_t, k_n, k_t, k_n)$. The reader will notice that the contact springs are oriented along the normal and tangential directions to each contact interface. For this reason, a local reference system has been defined for each interface (left and right). T is a transformation matrix of forces and displacements from the global (damper center of mass) to the local (i.e. damper contact points) reference system and viceversa. Similarly R is a rotation matrix from global to local reference system, used for the platforms DOFs. Both matrices are a function of the platform angles θ_L and θ_R .

If variation of forces and displacements are considered, Eq. A.2 becomes:

$$K_D \cdot \Delta Q_D = K_P \cdot \Delta Q_P \quad (\text{A.4})$$

where the inertial terms can be neglected as demonstrated in [54] and $\Delta F_{ED} = 0$ since the centrifugal force is a constant term. The damper displacement variation ΔQ_D is expressed as:

$$\Delta Q_D = K_D^{-1} \cdot K_P \cdot \Delta Q_P \quad (\text{A.5})$$

Then the vector of contact forces in global coordinate system at the platform contact points can be expressed as:

$$\Delta F = R' \cdot K_{local} (R - T \cdot K_D^{-1} \cdot K_P) \cdot \Delta Q_P \quad (\text{A.6})$$

Where $\Delta F = (\Delta H_L, \Delta V_L, \Delta H_R, \Delta V_R)'$ is the vector of contact forces on the two blade platforms. It is then possible to write:

$$\Delta F = K_I^* \cdot \Delta Q_P \quad (\text{A.7})$$

where K_I^* has the following structure:

$$K_I^* = \begin{bmatrix} K_I & -K_I \\ -K_I & K_I \end{bmatrix} = \begin{bmatrix} K_H & K_{HV} & -K_H & -K_{HV} \\ K_{HV} & K_V & -K_{HV} & -K_V \\ -K_H & -K_{HV} & K_H & K_{HV} \\ -K_{HV} & -K_V & K_{HV} & K_V \end{bmatrix} \quad (\text{A.8})$$

The matrix K_I is here termed the global platform-to-platform stiffness matrix and can be used to link a blade to a neighboring structure, be it an adjacent blade (real working conditions) or a ground platform (test rig condition). In case of pure in-phase motion only the vertical relative platform displacement is present and therefore only the K_V entry is of interest. Its analytical expression is:

$$K_V = \frac{-k_n k_t (2 \cos(\theta_R + \theta_L) - \cos(2\theta_R) - \cos(2\theta_L) + 2 \cos(\theta_R - \theta_L))}{[3k_n + 5k_t - 2k_n \cos(\theta_L + \theta_R) - 6k_t \cos(\theta_L + \theta_R) + (k_t - k_n) \cdot (\cos(4\theta_L) + \cos(2\theta_L - 2\theta_R) + \cos(2\theta_L + 2\theta_R) - 2 \cos(3\theta_L - \theta_R))]} \quad (\text{A.9})$$

Appendix A.1. Algorithm to identify the tangential contact stiffness

The procedure to estimate k_t is iterative.

1. Set the k_n value corresponding to CF under investigation (see Sect. 7.2 for further details):
2. Define an initial guess on the k_t value, k_t'
3. Compute $K_{V,num}$ (according to Eq. A.9) and compare it to $K_{V,meas}$ (see Fig. 13)
 - If $K_{V,num} \approx K_{V,meas}$, then $k_t = k_t'$
 - If $K_{V,num} \neq K_{V,meas}$, then update the initial guess k_t' accordingly. In this paper the new value of k_t' is obtained by multiplying the initial guess on k_t from point 2. by the factor $\frac{K_{V,meas}}{K_{V,num}}$. Other criteria are possible. Go back to Step 3.

References

- [1] B. D. Yang, J. J. Chen, C. H. Menq, Prediction of resonant response of shrouded blades with three-dimensional shroud constraint, *Journal of Engineering for Gas Turbines and Power* 121 (3) (1999) 523. doi:10.1115/1.2818504.
- [2] S. Yajie, H. Jie, S. Yingchun, Z. Zigen, Forced response analysis of shrouded blades by an alternating frequency/time domain method, in: *Volume 5: Marine Microturbines and Small Turbomachinery Oil and Gas Applications Structures and Dynamics, Parts A and B*, ASME, 2006. doi:10.1115/gt2006-90595.
- [3] J. Szwedowicz, C. Gibert, T. P. Sommer, R. Kellerer, Numerical and experimental damping assessment of a thin-walled friction damper in the rotating setup with high pressure turbine blades, *ASME. J. Eng. Gas Turbines Power* 130 (1) (2008) 012502–012502–10. doi:10.1115/1.2771240.
- [4] C. Siewert, L. Panning, J. Wallaschek, C. Richter, Multiharmonic forced response analysis of a turbine blading coupled by nonlinear contact forces, *Journal of Engineering for Gas Turbines and Power* 132 (8) (2010) 082501. doi:10.1115/1.4000266.
- [5] S. Zucca, C. M. Firrone, M. M. Gola, Numerical assessment of friction damping at turbine blade root joints by simultaneous calculation of the static and dynamic contact loads, *Nonlinear Dynamics* 67 (3) (2011) 1943–1955. doi:10.1007/s11071-011-0119-y.

- [6] W. Gu, Z. Xu, Y. Liu, A method to predict the non-linear vibratory response of bladed disc system with shrouded dampers, Proceedings of the Institution of Mechanical Engineers, Part C: Journal of Mechanical Engineering Science 226 (6) (2011) 1620–1632. doi:10.1177/0954406211424671.
- [7] M. Mitra, S. Zucca, B. Epureanu, Adaptive microslip projection for reduction of frictional and contact nonlinearities in shrouded blisks, Journal of Computational and Nonlinear Dynamics 11 (4) (2016) 041016. doi:10.1115/1.4033003.
- [8] S. M. Pourkiaee, S. Zucca, A reduced order model for nonlinear dynamics of mistuned bladed disks with shroud friction contacts, in: Volume 7C: Structures and Dynamics, ASME, 2018. doi:10.1115/gt2018-75223.
- [9] A. Hartung, H.-P. Hackenberg, M. Krack, J. Gross, T. Heinze, L. P. von Scheidt, Rig and engine validation of the non-linear forced response analysis performed by the tool OrAgL, in: Volume 7C: Structures and Dynamics, ASME, 2018. doi:10.1115/gt2018-75186.
- [10] B. Yang, M. C.H., Characterization of contact kinematics and application to the design of wedge dampers in turbomachinery blading: Part 2 – prediction of forced response and experimental verification., ASME J. Eng. Gas Turbines Power 120 (2) (1998) 418–423. doi:10.1115/1.2818139.
- [11] L. Panning, W. Sextro, K. Popp, Optimization of interblade friction damper design, in: Volume 4: Manufacturing Materials and Metallurgy Ceramics Structures and Dynamics Controls, Diagnostics and Instrumentation Education, ASME, 2000. doi:10.1115/2000-GT-0541.
- [12] L. Panning, W. Sextro, K. Popp, Spatial dynamics of tuned and mistuned bladed disks with cylindrical and wedge-shaped friction dampers, International Journal of Rotating Machinery 9 (3) (2003) 219–228. doi:10.1155/S1023621X03000198.
- [13] E. P. Petrov, D. J. Ewins, Advanced modeling of underplatform friction dampers for analysis of bladed disk vibration, Journal of Turbomachinery 129 (1) (2007) 143. doi:10.1115/1.2372775.
- [14] T. Berruti, C. Firrone, M. Pizzolante, M. Gola, Fatigue damage prevention on turbine blades: Study of underplatform damper shape, Key Eng Mat 347 (2007) 159–164. doi:10.4028/www.scientific.net/KEM.347.159.
- [15] T. Berruti, A test rig for the investigation of the dynamic response of a bladed disk with underplatform dampers, Mech. Re.Comm. 37 (6) (2010) 581–583. doi:10.1016/j.mechrescom.2010.07.008.
- [16] I. Sever, P. E.P., E. D.J., Experimental and numerical investigation of rotating bladed disk forced response using underplatform friction dampers, ASME J. Eng. Gas Turbines Power 130 (4) (2008) 042503–11. doi:10.1115/1.2903845.
- [17] C. M. Firrone, T. M. Berruti, M. M. Gola, On force control of an engine order-type excitation applied to a bladed disk with underplatform dampers, Journal of Vibration and Acoustics 135 (4) (2013) 041103. doi:10.1115/1.4023899.
- [18] D. Botto, C. Gastaldi, M. M. Gola, M. Umer, An experimental investigation of the dynamics of a blade with two under-platform dampers, Journal of Engineering for Gas Turbines and Power 140 (3) (2017) 032504. doi:10.1115/1.4037865.
- [19] L. Pesaresi, L. Salles, A. Jones, J. Green, C. Schwingshackl, Modelling the nonlinear behaviour of an underplatform damper test rig for turbine applications, Mechanical Systems and Signal Processing 85 (2017) 662–679.
- [20] K. Şanlıturk, D. Ewins, A. Stanbridge, Underplatform dampers for turbine blades: theoretical modelling, analysis and comparison with experimental data, J Eng Gas Turbine Power 123 (4) (2001) 919–929.
- [21] L. Panning, K. Popp, W. Sextro, F. Götting, A. Kayser, I. Wolter, Asymmetrical underplatform dampers in gas turbine bladings: Theory and application doi:10.1115/GT2004-53316.
- [22] S. Zucca, J. Borrajo, M. Gola, Forced response of bladed disks in cyclic symmetry with underplatform dampers, in: Volume 5: Marine Microturbines and Small Turbomachinery Oil and Gas Applications Structures and Dynamics, Parts A and B, ASME, 2006. doi:10.1115/GT2006-90785.
- [23] K.-H. Koh, J. H. Griffin, Dynamic behavior of spherical friction dampers and its implication to damper contact stiffness, Journal of Engineering for Gas Turbines and Power 129 (2) (2007) 511. doi:10.1115/1.2436547.
- [24] T. Berruti, C. Firrone, M. Gola, A test rig for noncontact traveling wave excitation of a bladed disk with underplatform dampers, Journal of Engineering for Gas Turbines and Power 133 (2011) 1–7.
- [25] C. Gastaldi, T. M. Berruti, M. M. Gola, Best practices for underplatform damper designers, Proceedings of the Institution of Mechanical Engineers, Part C: Journal of Mechanical Engineering Science 232 (7) (2018) 1221–1235. doi:10.1177/0954406217753654.
- [26] D. Botto, M. Umer, A novel test rig to investigate under-platform damper dynamics, Mechanical Systems and Signal Processing 100 (2018) 344–359.
- [27] M. Hls, L. P. von Scheidt, J. Wallaschek, Influence of geometric design parameters onto vibratory response and HCF safety for turbine blades with friction damper, in: Volume 7C: Structures and Dynamics, ASME, 2018. doi:10.1115/gt2018-75363.
- [28] C. Gastaldi, M. M. Gola, Criteria for best performance of pre-optimized solid dampers, in: ASME Turbo Expo 2018 Volume 7C: Structures and Dynamics, ASME, 2018. doi:10.1115/gt2018-75961.
- [29] E. Petrov, Explicit finite element models of friction dampers in forced response analysis of bladed disks, J Eng Gas Turb Power 130 (2) (2008) 022502. doi:10.1115/1.2772633.
- [30] M. Afzal, I. L. Arteaga, L. Kari, An analytical calculation of the jacobian matrix for 3d friction contact model applied to turbine blade shroud contact, Computers & Structures 177 (2016) 204–217. doi:10.1016/j.compstruc.2016.08.014.
- [31] C. Gastaldi, A. Fantetti, T. Berruti, Forced response prediction of turbine blades with flexible dampers: The impact of engineering modelling choices, Applied Sciences 8 (1) (2017) 34. doi:10.3390/app8010034.
- [32] A. Fantetti, C. Gastaldi, T. Berruti, Modeling and testing friction flexible dampers: Challenges and peculiarities, Experimental Techniques 42 (4) (2018) 407–419. doi:10.1007/s40799-018-0248-z.
- [33] J. Griffin, Friction damping of resonant stresses in gas turbine engine airfoils, Journal of Engineering for Power 102 (2) (1980) 329. doi:10.1115/1.3230256.
- [34] L. Panning, W. Sextro, K. Popp, Optimization of interblade friction damper design, in: N. Y. ASME (Ed.), Turbo Expo: Power for Land, Sea, and Air, Vol. 4, Munich, 2000. doi:10.1115/2000-GT-0541.
- [35] L. Panning, Symmetric and asymmetric underplatform dampers for turbine blades, PAMM 6 (1) (2006) 251–252. doi:10.1002/pamm.200610106.
- [36] C. Schwingshackl, E. Petrov, D. Ewins, Effects of contact interface parameters on vibration of turbine bladed disks with underplatform dampers, Journal of Engineering for Gas Turbines and Power 134 (3) (2012) 032507. doi:10.1115/1.4004721.

- [37] M. M. Gola, T. Liu, A direct experimental-numerical method for investigations of a laboratory under-platform damper behavior, *International Journal of Solids and Structures* 51 (25-26) (2014) 4245–4259.
- [38] M. Gola, C. Gastaldi, Understanding complexities in underplatform damper mechanics, in: *Volume 7A: Structures and Dynamics*, ASME International, 2014. doi:10.1115/GT2014-25240.
- [39] K.-H. Koh, J. H. Griffin, S. Filippi, A. Akay, Characterization of turbine blade friction dampers, *Journal of Engineering for Gas Turbines and Power* 127 (4) (2005) 856. doi:10.1115/1.1926312.
- [40] D. Botto, M. Lavella, M. M. Gola, Measurement of contact parameters of flat on flat contact surfaces at high temperature, in: *Volume 7: Structures and Dynamics, Parts A and B*, ASME International, 2012.
- [41] K. Y. Sanliturk, A. B. Stanbridge, D. J. Ewins, Friction dampers: measurement, modelling and application to blade vibration control, in: N. Y. ASME (Ed.), *Proc. Des. Eng. Conf.*, Vol. 3, Part B, Vol. 84, 1995, pp. 1377 – 1382.
- [42] S. Filippi, A. Akay, M. Gola, Measurements of tangential contact hysteresis during microslip, *Journal of Tribology* 126 (2004) 482–489.
- [43] C. Schwingshackl, E. Petrov, E. D.J., Validation of test rig measurements and prediction tools for friction interface modelling, in: N. Y. ASME (Ed.), *Turbo Expo: Power for Land, Sea, and Air*, Vol. 6, 2010. doi:10.1115/GT2010-23274.
- [44] D. Botto, M. Lavella, High temperature tribological study of cobalt-based coatings reinforced with different percentages of alumina, *Wear* 318 (1-2) (2014) 89–97. doi:10.1016/j.wear.2014.06.024.
- [45] C. Firrone, Measurement of the kinematics of two underplatform dampers with different geometry and comparison with numerical simulation, *Journal of Sound and Vibration* 323 (1-2) (2009) 313–333. doi:10.1016/j.jsv.2008.12.019.
- [46] J. Szwedowicz, M. Kissel, B. Ravindra, R. Kellerer, Estimation of contact stiffness and its role in the design of a friction damper, in: *Volume 4: Manufacturing Materials and Metallurgy Ceramics Structures and Dynamics Controls, Diagnostics and Instrumentation Education IGTI Scholar Award*, ASME, 2001. doi:10.1115/2001-GT-0290.
- [47] W. Sextro, K. Popp, I. Wolter, Improved reliability of bladed disks due to friction dampers, in: *ASME Turbo Expo: Power for Land, Sea, and Air*, Vol. 4 of *Manufacturing Materials and Metallurgy*, 1997. doi:10.1115/97-GT-189.
- [48] K. Y. Sanliturk, D. J. Ewins, A. B. Stanbridge, Underplatform dampers for turbine blades: Theoretical modeling, analysis, and comparison with experimental data, *ASME J. Eng. Gas Turbines Power* 123 (1998) 919 – 929. doi:10.1115/1.1385830.
- [49] A. Bessone, F. Toso, T. Berruti, Investigation on the dynamic response of blades with asymmetric under platform dampers, *ASME Turbo Expo 7B (GT2015-42597)*. doi:10.1115/GT2015-42597.
- [50] J. Szwedowicz, T. Secall-Wimmel, P. Dünck-Kerst, Damping performance of axial turbine stages with loosely assembled friction bolts: The nonlinear dynamic assessment, *Journal of Engineering for Gas Turbines and Power* 130 (3) (2008) 032505. doi:10.1115/1.2838998.
- [51] M. Gola, M. B. D. Santos, T. Liu, Design of a new test rig to evaluate underplatform damper performance, in: *ESDA 2010 - 24268*, 2010.
- [52] C. Gastaldi, M. Gola, Pre-optimization of asymmetrical underplatform dampers, *Journal of Engineering for Gas Turbines and Power* 139 (GTP-16-1229) (2016) 012504. doi:10.1115/1.4034191.
- [53] B. T. G. M. B. A. Gastaldi, C., Experimental investigation on real under-platform dampers: the impact of design and manufacturing, in: *Proceedings of ASME Turbo Expo 2019*, 2019.
- [54] C. Gastaldi, T. M. Berruti, M. M. Gola, A novel test rig for friction parameters measurement on underplatform dampers, *International Journal of Solids and Structures* doi:10.1016/j.ijsolstr.2019.08.030.
- [55] C. Gastaldi, M. Gola, A random sampling strategy for tuning contact parameters of underplatform dampers, in: *Volume 7B: Structures and Dynamics*, ASME International, 2015. doi:10.1115/GT2015-42834.
- [56] B. Yang, M. Chu, C. Menq, Stick-slip-separation analysis and non-linear stiffness and damping characterization of friction contacts having variable normal load, *Journal of Sound and Vibration* 210 (4) (1998) 461–481. doi:10.1006/jsvi.1997.1305.
- [57] D. Botto, M. Lavella, A numerical method to solve the normal and tangential contact problem of elastic bodies, *Wear* 330-331 (2015) 629–635. doi:10.1016/j.wear.2015.02.046.
- [58] T. Harris, M. Kotzalas, *Rolling Bearing Analysis*, 5th Edition, CRC Press, ISBN: 0849381673, 2006.
- [59] J. Brändlein, P. Eschmann, L. Hasbargen, K. Ball, *Ball and Roller Bearings: Theory, Design, and Application*, 3rd Edition, John Wiley and Sons, ISBN: 0471984523, 1999.
- [60] C. Gastaldi, M. Gola, On the relevance of a microslip contact model for under-platform dampers, *International Journal of Mechanical Sciences* 115-116 (2016) 145–156. doi:10.1016/j.ijmecsci.2016.06.015.
- [61] D. Li, D. Botto, C. Xu, T. Liu, M. Gola, A micro-slip friction modeling approach and its application in underplatform damper kinematics, *International Journal of Mechanical Sciences* 161-162 (2019) 105029. doi:10.1016/j.ijmecsci.2019.105029.